Machine learning of transient Structural-Thermal-Optical-Performance (STOP) models

Aleksandar Haber[a], John E. Draganov[b], and Michael Krainak[b]

[a]Department of Manufacturing and Mechanical Engineering Technology, College of Engineering Technology, Rochester Institute of Technology, 70 Lomb Memorial Dr., Rochester, NY 14623, USA

[b]Relative Dynamics Inc., 6401 Golden Triangle Dr. STE 201, Greenbelt, MD 20770, USA

ABSTRACT

In this paper, we investigate the feasibility of using machine learning methods for the estimation of Structural-Thermal-Optical-Performance (STOP) models of reflective optics. We use a model of a Newtonian telescope system to test machine learning methods. To generate the estimation data, we model and simulate a transient finite-element STOP model of the Newtonian telescope by using COMSOL Multiphysics and LiveLink for MATLAB software module. We use a feedforward neural network structure to estimate the STOP model. The inputs and outputs of the neural network correspond to the inputs and outputs of a Vector AutoRegressive eXogenous (VARX) model. Our results show that large-scale STOP dynamics can be effectively approximated by a low-order neural network model. Consequently, low-order VARX or state-space models can be reconstructed from the parameters of the estimated feedforward neural network, and used for the prediction, state estimation, and design of model-based controllers. We use the TensorFlow and Keras machine learning libraries and Python to estimate the feedforward neural network model. The developed COMSOL, MATLAB, and Python codes are available online.

Keywords: structural-thermal-optical-performance (STOP) analysis, telescopes, machine learning, system identification, adaptive optics

1. INTRODUCTION

The heating of optical elements and uneven temperature distributions across optical elements create structural deformations and thermally induced wavefront aberrations that can significantly limit the performance of optical systems. For example, these thermally-induced phenomena can degrade the performance of space and ground telescopes and instruments,[1–11] optical lithography machines,[12–19] high power lasers,[20–24] and other optical systems and devices.[25–28]

To analyze, predict, and correct for thermally induced wavefront aberrations, it is necessary to establish accurate transient models that mathematically relate absorbed heat fluxes or some other external effects that cause temperature gradients, with temperatures, deformations, and optical aberrations of the considered system. These models, which are often referred to as Structural Thermal Optical Performance (STOP) models, couple thermal, structural mechanics, and optics equations, as well as different boundary conditions and physical parameters. There are several challenges that need to be overcome in order to develop accurate STOP models. First, the parameters and other details of STOP models are often not known sufficiently accurately. This implies that STOP models often need to be estimated from observed experimental data. Secondly, STOP models are inherently large-dimensional. For example, finite-element STOP models simulated in this paper have in the order of 10^5 state variables. This number can be significantly larger (in the order of 10^6 or 10^7) for more complex and detailed STOP models. In addition, STOP models can have a number of model nonlinearities, such as nonlinear radiation and heat convection boundary conditions, that can significantly increase their mathematical complexity and greatly increase the necessary simulation time.

Further author information: (Send correspondence to A. H.)

A. H.: E-mail: aleksandar.haber@gmail.com; awhmet@rit.edu, Telephone: +1 585-475-5813

However, to predict the behavior or control weave-front aberrations we need to develop compact low-dimensional STOP models. In addition, to design high-performance model-based feedback control algorithms, the developed models should have appropriate mathematical forms, such as widely used Vector AutoRegressive eXogenous (VARX), transfer function, and state-space models.[29–34] There are two approaches for establishing low-order models. The first approach is based on model order reduction methods.[35,36] However, before the model order reduction techniques can be applied, we have to make sure that large-scale STOP models are experimentally validated. Tuning of parameters of large-scale STOP models that will ensure that model predictions match the observed experimental data is a computationally challenging and time-consuming task.[29] The second approach is based on a data-driven modeling paradigm. The main idea of the data-driven approaches is to collect the experimental data from the real system, and then to use this data and system identification or machine learning estimation methods to directly estimate low-order models.[15,30,33,37–39]

In this paper, we follow the data-driven modeling paradigm. We investigate the feasibility of using machine learning methods for the estimation of STOP models of reflective optics. We use a model of a Newtonian telescope system to test machine learning methods. To generate the estimation data, we model and simulate a transient finite-element STOP model of the Newtonian telescope by using COMSOL Multiphysics and LiveLink for MATLAB software module. We use a feedforward neural network structure to estimate the STOP model. The inputs and outputs of the neural network correspond to the inputs and outputs of a VARX model. Our results show that large-scale STOP dynamics can be effectively approximated by a low-order neural network model. Consequently, low-order VARX or state-space models can be reconstructed from the parameters of the estimated feedforward neural network, and can be used for the prediction, state estimation, and design of model-based controllers. We use the TensorFlow and Keras machine learning libraries and Python to estimate the feedforward neural network model. The developed COMSOL, MATLAB, and Python codes are available online.[40,41]

The modeling and validation frameworks investigated in this paper can be used for the development of adaptive optics systems for feedforward or feedback compensation of thermally-induced aberrations in optical systems.[42–50] In the accompanying publication,[51] we presented a system identification approach that complements and accompanies the approach presented in this paper. In,[51] we used subspace identification techniques to estimate STOP models of reflective optical systems. Both subspace identification and machine learning estimation approaches have their own merits. Experimental verification and comparison of these approaches is an important future research direction.

This paper is organized as follows. In Section 2, we briefly describe the system STOP model and present machine learning results. More details about this model can be found in the accompanying publication.[51] In Section 3 we present conclusions and briefly discuss future work directions.

2. STOP MODEL AND MACHINE LEARNING RESULTS

In this section, we first briefly describe the Newtonian telescope system that is used as a test case in this paper. We then present the machine learning approach and estimation results. Here it is important to emphasize that in the accompanying paper[51] we provided a detailed description of the system, together with ray tracing and STOP results. The interested reader is advised to consult[51] for the system's geometrical, optical, structural, and thermal parameters. Consequently, in this section, we only briefly describe the system and mainly focus on machine learning results. The codes used to perform STOP analysis, as well as machine learning Python codes, are given online.[40,41]

Figure 1 shows the structure of the system. The primary mirror is denoted by 1. The mirror support structure is denoted by 2. The image (focal) plane is denoted by 3. The secondary mirror is denoted by 4. The ray obstruction is denoted by 5. External heat flux disturbances are denoted by 6. The back side of the mirror contains an array of holes that can be used to place heaters or coolers, as well as thermocouples for observing the temperature field. These thermal actuators and sensors can be used to develop a feedback temperature control system whose purpose is to achieve both spatial and temporal thermal stability that will in turn ensure that wavefront aberrations and system structural deformations caused by external heat-flux disturbances are kept below the maximal allowed values. The array of holes is denoted by 7. To generate the STOP results for testing

the machine learning method, we use both heaters and heat-flux disturbances as inputs. The heater locations are denoted by blue circles 8 in Fig. 1.

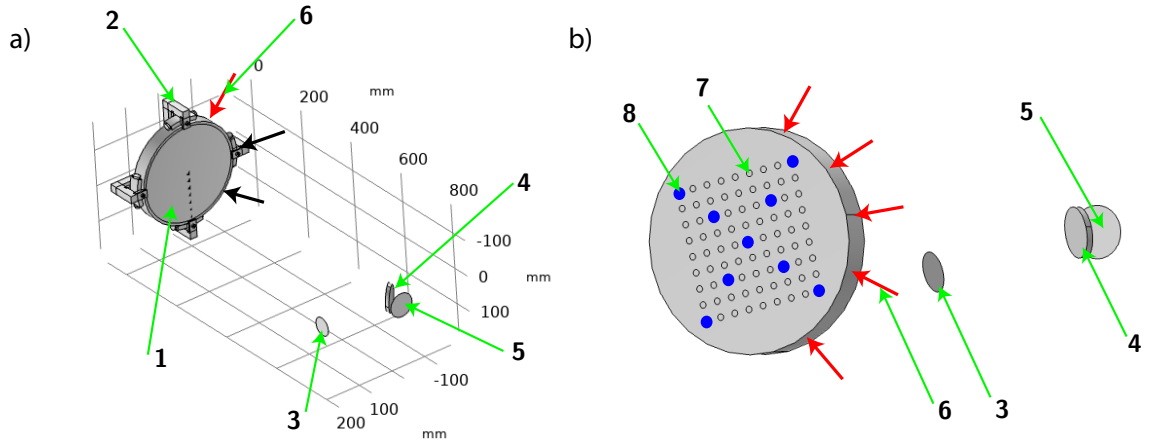

Figure 1. (a) Newtonian telescope system. (b) The back side of the mirror with arrows denoting the heat flux disturbances. Both (a) and (b): (1) primary mirror, (2) support structure, (3) image (focal) plane, (4) secondary mirror, (5) ray propagation obstruction, (6) external heat disturbances, (7) array of holes, and (8) locations of heaters

In the sequel, we present machine learning and model validation results. We aim at estimating a feedforward neural network structure whose inputs and outputs are identical to the inputs and outputs of Vector AutoRegressive eXogenous (VARX) models. This model structure was selected for two reasons. The first reason is that once the parameters of the neural network are estimated (learned), VARX or even state-space models can easily be constructed from the estimated parameters. Then, the constructed VARX or state-space models can be used for the design of advanced estimation and feedback control algorithms. The second reason is that it is easier to estimate feedforward neural networks than recurrent neural networks whose structure is similar to the structure of state-space models. Similarly to state-space models, recurrent neural networks have unknown and often unobservable states, and their estimation problems are inherently nonlinear and non-convex, often leading to suboptimal estimation results. Some progress has been made in estimating recurrent neural networks of dynamical systems. However, in the case of linear system estimation problems, recurrent neural network techniques are less effective than subspace identification techniques that are considered in the follow-up publication.[51]

The VARX model has the following form:

$$\mathbf{y}_k = \sum_{i=1}^{p} A_{k-i}\mathbf{y}_{k-i} + \sum_{i=1}^{p} B_{k-i}\mathbf{z}_{k-i} + \mathbf{w}_k \tag{1}$$

where the subscripts $k-i$, $i = 0, 1, 2, \ldots, p$, denote discrete-time instants, $\mathbf{y}_k \in \mathbb{R}^r$ is the output vector whose entries are the observed Zernike basis coefficients of wavefront aberrations at the focal (image) plane, $\mathbf{z}_{k-i} \in \mathbb{R}^{10}$ is the input vector whose entries are the power values generated by the control heaters and external heat-flux disturbances (denoted by 8 and 6, respectively, in Fig. 1), $A_{k-i} \in \mathbb{R}^{r\times r}$ and $B_{k-i} \in \mathbb{R}^{r\times 10}$ are the matrices multiplying the output and input vectors, respectively, p is the past window, and $\mathbf{w}_k \in \mathbb{R}^r$ is a zero-mean white-noise sequence. The vector $\mathbf{z}_{k-i}$ consists of the following scalar entries:

$$\mathbf{z}_{k-i} = \begin{bmatrix} u_{1,k-i} & u_{2,k-i} & \ldots & u_{9,k-i} & d_{1,k-i} \end{bmatrix}^T \tag{2}$$

where $u_{1,k-i}, u_{2,k-i}, \ldots, u_{9,k-i} \in \mathbb{R}$ are the control inputs (heat power generated by the heaters) at the discrete-time instant $k-i$ acting at locations denoted by blue circles in Fig. 1, and $d_{1,k-i} \in \mathbb{R}$ is the external disturbance denoted by 6 in Fig. 1. The feedforward neural network corresponding to the model (1) is compactly denoted by the following equation

$$\mathbf{y}_k = \mathcal{N}\big(\mathbf{y}_{k-1}, \mathbf{y}_{k-2}, \ldots, \mathbf{y}_{k-p}, \mathbf{z}_{k-1}, \mathbf{z}_{k-2}, \ldots, \mathbf{z}_{k-p}\big) + \mathbf{w}_k \tag{3}$$

where $\mathcal{N}(\,\cdot\,)$ is a compact notation for the feedforward neural network (neural network forward propagation operator).

A few comments related to the above-stated models are in order. First of all, we assumed that the past window p is the same for past outputs and past inputs. This is done to simplify the estimation problem and implementation complexity. Also, this modeling assumption produces good estimation results when tested on the simulated STOP model. However, there might be situations and scenarios in which we need to assume different past window values for inputs and outputs. Secondly, since this paper presents early results and numerical tests, and due to paper brevity, we assume that $\mathbf{w}_k$ is zero. This assumption is justified since we are using simulation results that substitute the experimental data. The performance validation of the used approach in the presence of real-experimental data is a future research direction. The experimental data is usually perturbed by stochastic noise. If the experimentally observed noise sequence is uncorrelated and zero mean, then the assumed neural network structure is appropriate. If that is not the case, then other model structures should be tested and used that can more accurately model the noise, such as for example, neural network structures whose inputs and outputs correspond to the inputs and outputs of vector autoregressive moving average exogenous models.

The machine learning problem can be stated as follows. *From the sequence of the input and output data* $\{\mathbf{y}_k, \mathbf{z}_k\}^{k=1,2,\ldots,N}$*, estimate the past window* p*, and a feedforward neural network model that for the past input* $\{\mathbf{z}_{k-1}, \mathbf{z}_{k-2}, \ldots, \mathbf{z}_{k-p}\}$ *and output* $\{\mathbf{y}_{k-1}, \mathbf{y}_{k-2}, \ldots, \mathbf{y}_{k-p}\}$ *data sets, predicts the value of* $\mathbf{y}_k$*.*

The model is estimated by performing the following steps.

Step 1: Simulate the system to obtain training, validation, and test data sets

To test the performance of the machine learning approach, we generate three data sets: training, validation, and test data sets. These data sets are generated by simulating the STOP model. Since the purpose of this paper is to numerically investigate the feasibility of using machine learning techniques for model estimation, we use simulation data that play the role of experimental data. This is a usual practice when developing estimation methods. That is, in the initial development phase, the method is tested on simulation data, and in the next phase, the method is tested on experimentally observed data collected from the real system. The experimental verification of the method developed in this paper is a future research direction.

We generate input sequences of control inputs and the disturbance as scaled binary pseudo-random numbers drawn from a uniform discrete distribution. Physically, this means that the control signals and disturbances are randomly turned off and on during the data-collection time interval. These types of input signals produce, piston, horizontal tilt, and defocus aberrations shown in panels (a) of Figs. 4, 5, and 6. There are only three dominant Zernike modes (coefficients) produced by these input signals. The magnitudes of other Zernike modes are at least 10-100 times smaller. Consequently, we select $r = 3$ in our simulations (r is the dimension of the output vector $\mathbf{y}_k$). We can also include additional Zernike terms if it is necessary to predict them. However, this will create some difficulties in estimating the model, since in that case, the outputs will have significantly different magnitudes. There are approaches for dealing with this issue, however, for paper brevity, we do not incorporate them in our estimation approach.

Here it should be emphasized that three statistically independent input sets are generated for simulating training, validation, and test data sets. This is done in order to ensure that the outputs of the training, validation and test data sets are different.[52] We assume a total simulation time of $9 \cdot 10^4$ seconds with the step size of 300 seconds. This produces 301 data samples. In practice, it is time-consuming to generate data sets with larger numbers of samples, since simulations of STOP models take a significant amount of time. STOP simulations in this paper are performed on a Dell workstation computer with 64 GB RAM, and an Intel i9-10900 CPU (2.80 GHz with 10 cores and 20 logical processors). It takes at least 6 hours of simulation time for a medium-size discretization mesh to obtain a single data set on this computer. The simulation of STOP models with denser discretization meshes or the simulation of more detailed STOP models can take days if not weeks to complete.

We use LiveLink for MATLAB COMSOL module to simulate the STOP model and obtain the data sets. The developed codes are available online.[41]

Step 2: Form the input-output data matrices and define the neural network

Once the input-output data sets are collected, we form data matrices. The structure of the neural network and the VARX models imply that in order to predict $\mathbf{y}_k$, we need to use the past input $\{\mathbf{z}_{k-1}, \mathbf{z}_{k-2}, \ldots, \mathbf{z}_{k-p}\}$ and past output $\{\mathbf{y}_{k-1}, \mathbf{y}_{k-2}, \ldots, \mathbf{y}_{k-p}\}$ data sets. This implies that the input and output data matrices for model learning (estimation) should be formed as follows:

$$\mathbf{U} = \begin{bmatrix} \mathbf{z}_0^T & \mathbf{z}_1^T & \cdots & \mathbf{z}_{p-1}^T & \mathbf{y}_0^T & \mathbf{y}_1^T & \cdots & \mathbf{y}_{p-1}^T \\ \mathbf{z}_1^T & \mathbf{z}_2^T & & \mathbf{z}_p^T & \mathbf{y}_1^T & \mathbf{y}_2^T & \cdots & \mathbf{y}_p^T \\ \vdots & \vdots & & \vdots & \vdots & \vdots & \cdots & \vdots \\ \mathbf{z}_{N-p}^T & \mathbf{z}_{N-p+1}^T & \cdots & \mathbf{z}_{N-1}^T & \mathbf{y}_{N-p}^T & \mathbf{y}_{N-p+1}^T & \cdots & \mathbf{y}_{N-1}^T \end{bmatrix}, \mathbf{Y} = \begin{bmatrix} \mathbf{y}_p^T \\ \mathbf{y}_{p+1}^T \\ \vdots \\ \mathbf{y}_N^T \end{bmatrix} \tag{4}$$

where $\mathbf{U} \in \mathbb{R}^{(N-p+1)\times p(10+r)}$ is the machine learning input data matrix and $\mathbf{Y} \in \mathbb{R}^{(N-p+1)\times r}$ is the machine learning output data matrix. Every row of the matrix U is used to predict the corresponding row of the matrix Y. That is, the rows of the matrix U should be used as inputs and the rows of Y should be used as outputs of the neural network. Consequently, during the network training (learning) process, we present to the network every row of the matrix U as input data and the corresponding row of the matrix Y as the output data. This implies that the neural network input layer should be composed of $p(10 + r)$ nodes (number of columns of the matrix U) and the output layer should be composed of r nodes (the number of columns of the matrix Y). The number of internal layers is a tuning variable that should be determined. Our numerical results show that the neural network with only input and output layers is able to accurately predict the system outputs that consist of 3 dominant Zernike coefficients (piston, horizontal tilt, and defocus). In all layers, we use linear activation functions and we set bias terms to zero. In future work, we will also explore nonlinear activation functions and networks with internal layers that can be useful for estimating more detailed STOP models or models with more output Zernike modes. For $p = 10$ (this is an estimated value of the parameter p), the network has 399 trainable parameters.

Step 3: Model estimation and tests

We use the TensorFlow and Keras Python libraries to estimate the model. The developed Python codes are provided online.[40] The first step is to estimate the past window p. First, we estimate a series of models starting from $p = 2$ until $p = 24$. For every value of the past window, we use both training and validation data sets to train the model. We use the mean square error as a loss function during training. To minimize the loss function, we use the Root Mean Square Propagation (RMSProp) optimization method.[52] The training data is used to fit the model parameters, and the validation data is used during training to validate (evaluate) the model prediction on the data set that is not used for training. The validation is performed after every training epoch. The model parameters that produce the smallest validation error are selected and stored. This model is referred to as the *trained model*. This type of training that is based on both training and validation data sets is widely used in the machine learning community.[52] We have a single trained model for every value of the past window p and overall, this procedure produces 24 trained models.

Training and validation curves are given in Fig. 2 for the model with the past window of $p = 10$. From Fig. 2 we see that the overfitting phenomenon is not occurring during the training process since the validation loss curve is following the training loss curve.

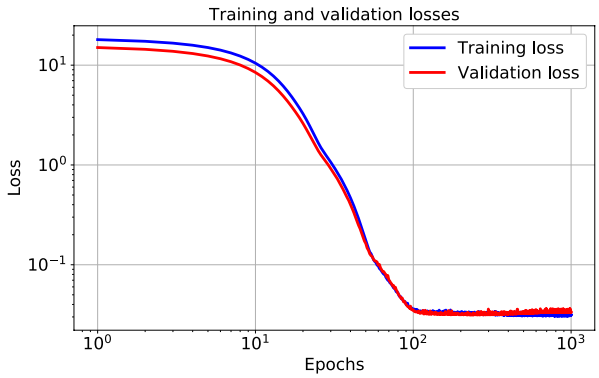

Figure 2. Training and validation loss curves obtained for the past window $p = 10$.

Once the trained models are obtained, we need to select the optimal value of p that produces the final model. That is, we need to select the most optimal model from the set of trained models. We select the final model by using the test data set. Using the inputs from the test data set, we can simulate the trained models to obtain closed-loop and open-loop predictions that are defined in the sequel. The closed-loop prediction of the output $\mathbf{y}_k$, denoted by $\hat{\mathbf{y}}_k$, is computed by forward propagation of the trained model:

$$\hat{\mathbf{y}}_k = \mathcal{N}\big(\mathbf{y}_{k-1}, \mathbf{y}_{k-2}, \ldots, \mathbf{y}_{k-p}, \mathbf{z}_{k-1}, \mathbf{z}_{k-2}, \ldots, \mathbf{z}_{k-p}\big) \tag{5}$$

where $\mathbf{y}_{k-1}, \mathbf{y}_{k-2}, \ldots, \mathbf{y}_{k-p}$ and $\mathbf{z}_{k-1}, \mathbf{z}_{k-2}, \ldots, \mathbf{z}_{k-p}$ are the outputs and inputs from the test data set. The open-loop prediction is performed as follows:

$$\tilde{\mathbf{y}}_k = \mathcal{N}\big(\tilde{\mathbf{y}}_{k-1}, \tilde{\mathbf{y}}_{k-2}, \ldots, \tilde{\mathbf{y}}_{k-p}, \mathbf{z}_{k-1}, \mathbf{z}_{k-2}, \ldots, \mathbf{z}_{k-p}\big) \tag{6}$$

where $\tilde{\mathbf{y}}_k$ is the notation used for the open-loop prediction. That is, in open-loop prediction, the predicted output is computed on the basis of the past open-loop output predictions and past inputs from the test data set. We quantify the open-loop and closed-loop prediction performances by computing relative prediction errors defined in the sequel. The open-loop relative prediction error $e_{\mathrm{OL}} \in \mathbb{R}$ and closed-loop relative prediction error $e_{\mathrm{CL}} \in \mathbb{R}$ are computed as follows:

$$e_{\mathrm{OL}} = \frac{\|\mathbf{e}_{\mathrm{OL}}\|_2}{\|\mathbf{y}\|_2}, \quad \mathbf{e}_{\mathrm{OL}} = \tilde{\mathbf{y}} - \mathbf{y} \tag{7}$$

$$e_{\mathrm{CL}} = \frac{\|\mathbf{e}_{\mathrm{CL}}\|_2}{\|\mathbf{y}\|_2}, \quad \mathbf{e}_{\mathrm{CL}} = \hat{\mathbf{y}} - \mathbf{y} \tag{8}$$

where $\mathbf{y}$, $\hat{\mathbf{y}}$, and $\tilde{\mathbf{y}}$ are the vector of sequences defined as follows

$$\mathbf{y} = \begin{bmatrix} \mathbf{y}_p \\ \mathbf{y}_{p+1} \\ \vdots \\ \mathbf{y}_N \end{bmatrix}, \quad \hat{\mathbf{y}} = \begin{bmatrix} \hat{\mathbf{y}}_p \\ \hat{\mathbf{y}}_{p+1} \\ \vdots \\ \hat{\mathbf{y}}_N \end{bmatrix}, \quad \tilde{\mathbf{y}} = \begin{bmatrix} \tilde{\mathbf{y}}_p \\ \tilde{\mathbf{y}}_{p+1} \\ \vdots \\ \tilde{\mathbf{y}}_N \end{bmatrix} \tag{9}$$

If we are mainly interested in open-loop prediction, then the final model should be selected on the basis of the open-loop prediction performance. In that case, the final model is selected as the trained model that produces the smallest open-loop relative prediction error. On the other hand, if the closed-loop prediction performance is used to evaluate the model quality, then the final model is selected as the trained model that produces the smallest closed-loop relative prediction error. Often, the open-loop and closed-loop relative prediction errors will be minimized for the same final model, that is, for the same value of p.

Figure 3(a) shows the open-loop and closed-loop relative prediction errors of the trained models as functions of the past window p. From this figure, we can observe that the optimal value of p that produces the smallest

open-loop and closed-loop relative prediction errors is $p = 10$. Consequently, we select the final model as the trained model obtained for $p = 10$. Figure 3(b) shows the correlation values of the entries of the open-loop error vector (7) corresponding to the defocus term. This graph shows the autocorrelation of the open-loop error of predicting the defocus term. Dashed red lines denote the bounds of an interval for testing the white-noise hypothesis of the open-loop error. If more than 95% of the correlation values are inside of the bounds, then the prediction error sequence has a white noise property. This is the residual test that is used to evaluate the quality of the estimated model. Closer the residual sequence to white noise, more information available in the estimation data is captured by the model, and consequently, the model quality is better. We can see that for smaller values of lags, there is a non-negligible correlation. After that, the correlation values are within the bounds. Consequently, there is still some space for improving the model quality. This can be potentially achieved by using different model structures, nonlinear activation functions, or including more internal layers in the neural network. However, as it will be shown in the sequel, despite this, the estimated model has an excellent prediction performance.

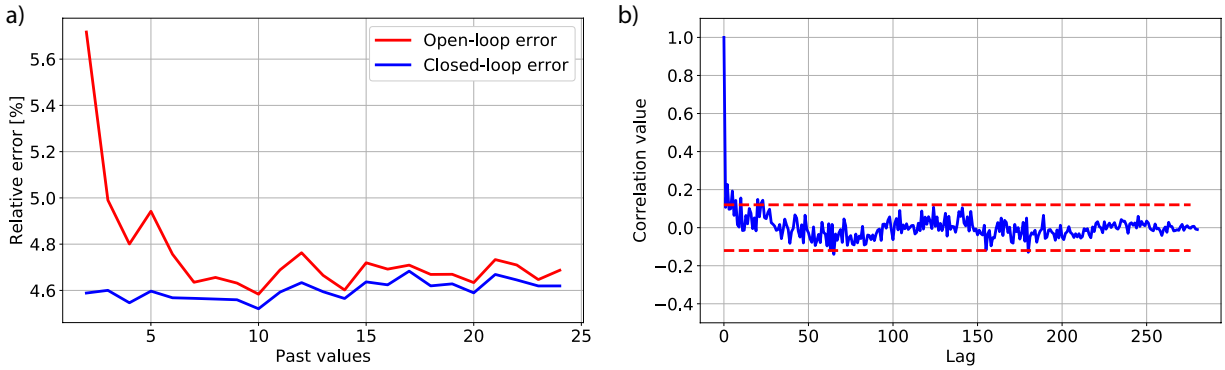

Figure 3. (a) Open-loop and closed-loop relative prediction errors of trained models as functions of the past window p. (b) Correlation values of the entries of the open-loop error vector (7) corresponding to the defocus term. The results are generated for the past window $p = 10$. The dashed red lines denote the bounds of the interval for testing the white-noise hypothesis of the open-loop error.

Figures 4,5, and 6, show the open-loop and closed-loop prediction performances for piston, horizontal tilt, and defocus terms, respectively. These results are generated for the final model (obtained for $p = 10$). We can observe that the prediction performance is very good for piston and defocus coefficients. The prediction performance for the horizontal tilt is worse. There are several potential reasons for that. First of all, there is approximately a factor of 10 magnitude difference between piston and defocus coefficients on one side, and horizontal tilt on the other side. This implies that a proper data scaling or weighting of the loss function need to be introduced. Then, we are using a neural network structure with only two layers without hidden layers and with linear activation functions. Networks with more layers and with nonlinear activation functions will most likely produce better results. Finally, we can observe that the time behavior of the horizontal tilt is highly oscillatory, implying that the eigenvalues of the system are close to the unit circle. This fact raises an identifiability issue that needs to be carefully addressed.

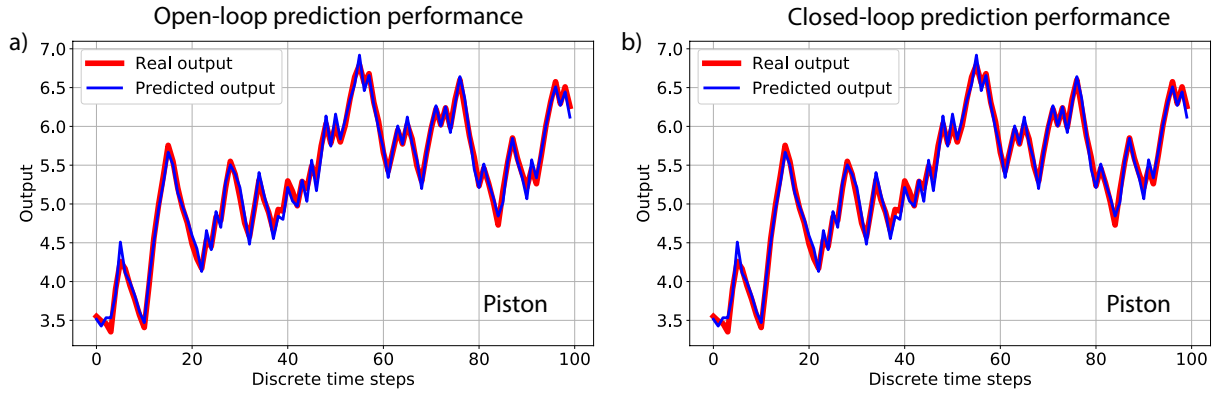

Figure 4. (a) Open-loop and (b) closed-loop prediction performance of the final model (obtained for $p = 10$). The results show the piston coefficient.

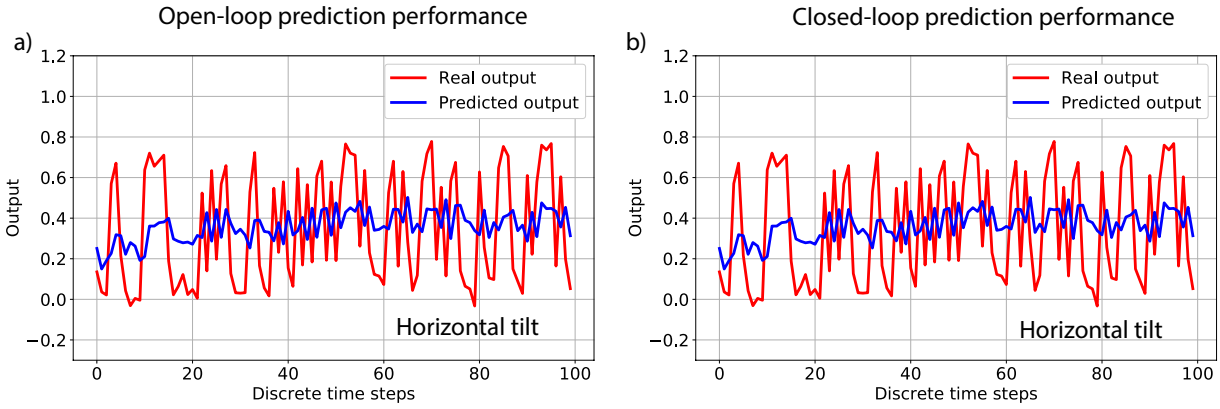

Figure 5. (a) Open-loop and (b) closed-loop prediction performance of the final model (obtained for $p = 10$). The results show the horizontal tilt coefficient.

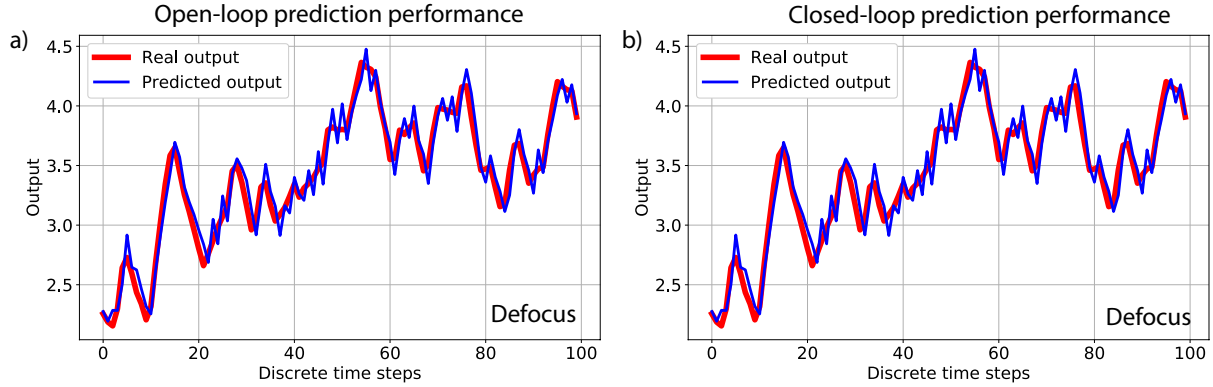

Figure 6. (a) Open-loop and (b) closed-loop prediction performance of the final model (obtained for $p = 10$). The results show the defocus coefficient.

3. CONCLUSION AND FUTURE WORK

In this paper, we investigated the feasibility of using machine learning techniques for estimating low-order Structural Thermal Optical Performance (STOP) models of a Newtonian telescope system. We demonstrated that

we can estimate a low-order STOP model that can accurately predict dominant Zernike coefficients of wavefront aberrations. The developed estimation and model validation methodologies can be used to develop advanced feedback controllers and observers for controlling wavefront aberrations in a number of optical systems, such as ground and space telescopes, optical instruments requiring thermal stability, optical lithography machines, etc. Also, the developed model can be combined with adaptive optics systems to compensate for thermally induced wave-front aberrations. Future research directions should be focused on improving the estimation performance by using feedforward neural networks with internal layers, nonlinear activation functions, and recurrent neural networks.

REFERENCES

[1] Brooks, T. E. and Stahl, H. P., "Precision thermal control technology to enable thermally stable telescopes," *J. Astron. Telesc. Instrum. Syst.* **8**(2), 024001 (2022).

[2] Havey Jr, K., Martens, B., Hahm, T., Voyer, P., and Shomper, M., "Challenges and benefits to achieving sub-millikelvin thermal control stability on large space observatories," in [*Proc. SPIE*], **11116**, 1111607 (2019).

[3] Segato, E., Da Deppo, V., Debei, S., Naletto, G., Cremonese, G., and Flamini, E., "Method for studying the effects of thermal deformations on optical systems for space application," *Appl. Optics* **50**(18), 2836–2845 (2011).

[4] Brooks, T. E., "Predictive thermal control applied to HabEx," in [*Proc. SPIE*], **10398**, 1039814 (2017).

[5] Zhang, G., Zhao, H., Chen, Y., Zhang, G., Zhang, Z., Peng, J., Zhao, Z., and Yan, A., "Optimization thermal design method for space cameras based on thermo-optical analysis and Taguchi method," *Opt. Eng.* **59**(7), 075101 (2020).

[6] Stahl, H. P., "Advanced ultraviolet, optical, and infrared mirror technology development for very large space telescopes," *J. Astron. Telesc. Instrum. Syst.* **6**(2), 025001 (2020).

[7] Stahl, H. P., Brooks, T. E., Effinger, M., Eng, R., and Young, R., "Predictive Thermal Control (PTC) technology to enable thermally stable telescopes: year three status," in [*Proc. SPIE*], **11487**, 114870T (2020).

[8] Banyal, R. K., Ravindra, B., and Chatterjee, S., "Opto-thermal analysis of a lightweighted mirror for solar telescope," *Opt. Express* **21**(6), 7065–7081 (2013).

[9] Buleri, C., Kehoe, M., Lukashin, C., Jackson, T., Beckman, J., Curtis, A., Edwards, B., Owen, T., Phenis, A., and Stebbins, M., "Structural, thermal, and optical performance (STOP) analysis of the NASA ARCSTONE instruments," in [*Proc. SPIE*], **10925**, 1092503 (2019).

[10] Blaurock, C., McGinnis, M., Kim, K., and Mosier, G. E., "Structural-thermal-optical performance (STOP) sensitivity analysis for the James Webb Space Telescope," in [*Proc. SPIE*], **5867**, 58670V (2005).

[11] Gu, N., Li, C., Cheng, Y., and Rao, C., "Thermal control for light-weighted primary mirrors of large ground-based solar telescopes," *J. Astron. Telesc. Instrum. Syst.* **5**(1), 014005 (2019).

[12] Zhao, L., Dong, L., Yu, X., Li, P., and Qiao, Y., "Active lens for thermal aberration compensation in lithography lens," *Appl. Optics* **57**(29), 8654–8663 (2018).

[13] Bikcora, C., Weiland, S., and Coene, W. M. J., "Thermal deformation prediction in reticles for extreme ultraviolet lithography based on a measurement-dependent low-order model," *IEEE Trans. Semicond. Manuf.* **27**(1), 104–117 (2014).

[14] Heertjes, M. F., Butler, H., Dirkx, N. J., van der Meulen, S. H., Ahlawat, R., O'Brien, K., Simonelli, J., Teng, K. T., and Zhao, Y., "Control of wafer scanners: methods and developments," in [*Proceedings of American Control Conference*], 3686–3703, IEEE (2020).

[15] Haber, A., Polo, A., Ravensbergen, S., Urbach, H. P., and Verhaegen, M., "Identification of a dynamical model of a thermally actuated deformable mirror," *Opt. Lett.* **38**(16), 3061–3064 (2013).

[16] Bikcora, C., van Veelen, M., Weiland, S., and Coene, W. M. J., "Lens heating induced aberration prediction via nonlinear kalman filters," *IEEE Trans. Semicond. Manuf.* **25**(3), 384–393 (2012).

[17] Choi, J. P., Park, T., Nam, Y. S., Kang, Y. S., Park, C.-H., Park, K.-Y., Ryu, C.-H., Huang, W., and Baik, K.-H., "Lens heating impact analysis and controls for critical device layers by computational method," in [*Proc. SPIE*], **8683**, 553–560 (2013).

[18] Ravensbergen, S. K., Rosielle, P. C. J. N., and Steinbuch, M., "Deformable mirrors with thermo-mechanical actuators for extreme ultraviolet lithography: design, realization and validation," *Precis. Eng.* **37**(2), 353–363 (2013).

[19] Haber, A., Polo, A., Maj, I., Pereira, S. F., Urbach, H. P., and Verhaegen, M., "Predictive control of thermally induced wavefront aberrations," *Opt. Express* **21**(18), 21530–21541 (2013).

[20] Wyss, E., Roth, M., Graf, T., and Weber, H. P., "Thermooptical compensation methods for high-power lasers," *IEEE J. Quantum Electron.* **38**(12), 1620–1628 (2002).

[21] Schmidt, K., Beirow, F., Böhm, M., Graf, T., Ahmed, M. A., and Sawodny, O., "Towards adaptive high-power lasers: Model-based control and disturbance compensation using moving horizon estimators," *Mechatronics* **71**, 102441 (2020).

[22] Lyu, C. and Zhan, R., "Stop model development and analysis of an optical collimation system for a tactical high-energy laser weapon," *Appl. Opt.* **60**(13), 3596–3603 (2021).

[23] Schmidt, K., Graf, T., Ahmed, M. A., and Sawodny, O., "Energy-optimal disturbance feedforward control for constrained deformable mirrors with thermoelastic actuation," in [*Proceedings of IEEE International Conference on Systems, Man and Cybernetics*], 107–112, IEEE (2019).

[24] Abt, F., Hess, A., and Dausinger, F., "Temporal behaviour of the focal shift of beam forming optics for high power single mode lasers," in [*Proceedings of International Congress on Applications of Lasers & Electro-Optics*], **2008**(1), 561–568, Laser Institute of America (2008).

[25] Zhao, C., Degallaix, J., Ju, L., Fan, Y., Blair, D. G., Slagmolen, B. J. J., Gray, M. B., Lowry, C. M. M., McClelland, D. E., Hosken, D. J., Mudge, D., Brooks, A., Munich, J., Veitch, P. J., Barton, M. A., and Billingsley, G., "Compensation of strong thermal lensing in high-optical-power cavities," *Phys. Rev. Lett.* **96**(23), 231101 (2006).

[26] Loriette, V. and Boccara, C., "Absorption of low-loss optical materials measured at 1064 nm by a position-modulated collinear photothermal detection technique," *Appl. Optics* **42**(4), 649–656 (2003).

[27] Ramette, J., Kasprzack, M., Brooks, A., Blair, C., Wang, H., and Heintze, M., "Analytical model for ring heater thermal compensation in the advanced laser interferometer gravitational-wave observatory," *Appl. Opt.* **55**(10), 2619–2625 (2016).

[28] Dobek, K., "Thermal lensing: outside of the lasing medium," *Appl. Phys. B* **128**(2), 1–21 (2022).

[29] Haber, A., Draganov, J. E., Heesh, K., Cadena, J., and Krainak, M., "Modeling, experimental validation, and model order reduction of mirror thermal dynamics," *Opt. Express* **29**(15), 24508–24524 (2021).

[30] Verhaegen, M. and Verdult, V., [*Filtering and System Identification: a Least Squares Approach*], Cambridge (2007).

[31] Haber, A., "Subspace identification of temperature dynamics," *arXiv preprint arXiv:1908.02379* (2019).

[32] Chiuso, A., Muradore, R., and Marchetti, E., "Dynamic calibration of adaptive optics systems: A system identification approach," *IEEE Trans. Control Syst. Technol.* **18**(3), 705–713 (2009).

[33] Haber, A., Draganov, J. E., Heesh, K., Tesch, J., and Krainak, M., "Modeling and system identification of transient STOP models of optical systems," *Opt. Express* **28**(26), 39250–39265 (2020).

[34] Haber, A., Pecora, F., Chowdhury, M. U., and Summerville, M., "Identification of temperature dynamics using subspace and machine learning techniques," in [*Proceedings of ASME Dynamic Systems and Control Conference*], **59155**, V002T24A003, ASME (2019).

[35] Castagnotto, A., Varona, M. C., Jeschek, L., and Lohmann, B., "sss & sssMOR: Analysis and reduction of large-scale dynamic systems in MATLAB," *Automatisierungstechnik* **65**(2), 134–150 (2017).

[36] Schilders, W. H. A., Van der Vorst, H. A., and Rommes, J., [*Model Order Reduction: Theory, Research Aspects and Applications*], vol. 13, Springer (2008).

[37] Haber, A., "Steady-state control and machine learning of large-scale deformable mirror models," *arXiv preprint arXiv:1911.07456* (2019).

[38] Huang, L., Ma, X., Bian, Q., Li, T., Zhou, C., and Gong, M., "High-precision system identification method for a deformable mirror in wavefront control," *Appl. Opt.* **54**(14), 4313–4317 (2015).

[39] Haber, A. and Verhaegen, M., "Subspace identification of large-scale interconnected systems," *IEEE Trans. Automat. Contr.* **59**(10), 2754–2759 (2014).

[40] Haber, A., "Python and COMSOL Livelink for MATLAB codes for machine learning of structural-thermal-optical performance (STOP) models," (2022). [retrieved 24 July 2022], https://github.com/AleksandarHaber/Machine-learning-of-transient-structural-thermal-optical-peformance-STOP-models.

[41] Haber, A., "Codes for simulating transient structural thermal optical performance (STOP) analysis of Newtonian telescope," (2022). [retrieved 17 July 2022], https://github.com/AleksandarHaber/transient-structural-thermal-optical-performance-STOP-analysis-of-reflective-optics.

[42] Haber, A. and Bifano, T., "Dual-update data-driven control of deformable mirrors using Walsh basis functions," *JOSA A* **39**(3), 459–469 (2022).

[43] Roddier, F., [*Adaptive Optics In Astronomy*], Cambridge (1999).

[44] Haber, A., Polo, A., Smith, C. S., Pereira, S. F., Urbach, P., and Verhaegen, M., "Iterative learning control of a membrane deformable mirror for optimal wavefront correction," *Appl. Opt.* **52**(11), 2363–2373 (2013).

[45] Bonora, S. and Poletto, L., "Push-pull membrane mirrors for adaptive optics.," *Opt. Express* **14**(25), 11935–11944 (2006).

[46] Polo, A., Haber, A., Pereira, S. F., Verhaegen, M., and Urbach, H. P., "Linear phase retrieval for real-time adaptive optics," *J. Eur. Opt. Soc.-Rapid* **8**(13070) (2013).

[47] Tyson, R., [*Principles of Adaptive Optics*], CRC (2015).

[48] Polo, A., Haber, A., Pereira, S. F., Verhaegen, M., and Urbach, H. P., "An innovative and efficient method to control the shape of push-pull membrane deformable mirror," *Opt. Express* **20**, 27922–27932 (Dec 2012).

[49] Vogel, C., Tyler, G., Lu, Y., Bifano, T., Conan, R., and Blain, C., "Modeling and parameter estimation for point-actuated continuous-facesheet deformable mirrors," *JOSA A* **27**(11), A56–A63 (2010).

[50] Haber, A. and Bifano, T., "General approach to precise deformable mirror control," *Opt. Express* **29**(21), 33741–33759 (2021).

[51] Haber, A., Draganov, J. E., and Krainak, M., "Subspace identification of low-dimensional Structural-Thermal-Optical-Performance (STOP) models of reflective optics," in [*Proc. SPIE, to be published*], (2022).

[52] Chollet, F., [*Deep learning with Python*], Simon and Schuster (2021).